1521-009X/12/4001-25–31$25.00
DRUG METABOLISM AND DISPOSITION
Vol. 40, No. 1

42283/3735130
DMD 40:25–31, 2012

In Vitro Glucuronidation of the Antibacterial Triclocarban and Its Oxidative Metabolites[S]

N. H. Schebb, B. Franze, R. Maul, A. Ranganathan, and B. D. Hammock

University of Veterinary Medicine Hannover, Institute for Food Toxicology and Chemical Analysis, Hannover, Germany (N.H.S.); University of California, Davis, Department of Entomology and Cancer Research Center, Davis, California (B.F., A.R., B.D.H.); and BAM Federal Institute for Materials Research and Testing, Division of Organic Chemical Analysis & Reference Materials, Berlin, Germany (R.M.)

Received August 10, 2011; accepted September 27, 2011

ABSTRACT:

Triclocarban (3,4,4′-trichlorocarbanilide; TCC) is widely used as an antibacterial in bar soaps. During use of these soaps, a significant portion of TCC is absorbed by humans. For the elimination from the body, glucuronidation plays a key role in both biliary and renal clearance. To investigate this metabolic pathway, we performed microsomal incubations of TCC and its hydroxylated metabolites 2′-OH-TCC, 3′-OH-TCC, and 6-OH-TCC. Using a new liquid chromatography-UV-mass spectrometry method, we could show a rapid glucuronidation for all OH-TCCs by the uridine-5′-diphosphate-glucuronosyltransferases (UGT) present in liver microsomes of humans (HLM), cynomolgus monkeys (CLM), rats (RLM), and mice (MLM). Among the tested human UGT isoforms, UGT1A7, UGT1A8, and UGT1A9 showed the highest activity for the conjugation of hydroxylated TCC metabolites followed by UGT1A1, UGT1A3, and UGT1A10. Due to this broad pattern of active UGTs, OH-TCCs can be efficiently glucuronidated in various tissues, as shown for microsomes from human kidney (HKM) and intestine (HIM). The major renal metabolites in humans, TCC-*N*-glucuronide and TCC-*N*′-glucuronide, were formed at very low conversion rates (<1%) by microsomal incubations. Low amounts of *N*-glucuronides were generated by HLM, HIM, and HKM, as well as by MLM and CLM, but not by RLM, according to the observed species specificity of this metabolic pathway. Among the human UGT isoforms, only UGT1A9 had activity for the N-glucuronidation of TCC. These results present an anomaly where in vivo the predominant urinary metabolites of TCC are *N* and *N*′-glucuronides, but these compounds are slowly produced in vitro.

Introduction

Triclocarban (3,4,4′-trichlorocarbanilide; TCC) (Fig. 1) is widely used as an antibacterial agent in bar soaps in the United States. It can generally be added to rinse-off personal care products in the United States and European Union in concentrations up to 1.5% [European Food Safety Authority, Opinion on Triclocarban (2005), Scientific Committee on Consumer Products, http://ec.europa.eu/health/ph_risk/committees/04_sccp/docs/sccp_o_016.pdf; Ahn et al., 2008]. Due to its widespread use and environmental persistence, TCC was detected in surface waters up to microgram per liter scale (Halden and Paull, 2005; Sapkota et al., 2007). Much higher levels of up to 0.44 g/kg were found in sludge, as shown in the Targeted National Sewage Sludge Survey, published by the U.S. Environmental Protection Agency in 2009. Moreover, TCC strongly accumulates in aquatic organisms such as algae (*Cladophora* spp.) and snails (log bioconcentration factor 3.2–3.4) (Coogan et al., 2007; Coogan and La Point, 2008).

Several studies have indicated that a significant portion of TCC in soaps is percutaneously absorbed by humans during and after showering (Scharpf et al., 1975; Schebb et al., 2011c). Approximately 0.4% of the applied TCC is found in the excreta and, thus, was absorbed and systemically available. Moreover, it has to be assumed that TCC from contaminated drinking water or food will be extensively absorbed, because TCC shows a high bioavailability after oral dosing (Hiles, 1977; Jeffcoat et al., 1977; Hiles and Birch, 1978a; Warren et al., 1978). These TCC exposures might be relevant to human health, because of unintended biological activities of TCC. By enhancing the action of steroids, TCC may have the potential to act as an endocrine disruptor (Ahn et al., 2008; Chen et al., 2008). Moreover, we recently showed that TCC inhibits the enzyme-soluble epoxide hydrolase, with an in vitro potency (IC_{50} 24 ± 5 nM) (Morisseau et al., 2009; Schebb et al., 2011b,c) comparable with synthetic inhibitors, which proved to alter the biological regulation of inflammation, pain, and blood pressure in vivo (Inceoglu et al., 2006; Imig and Hammock, 2009; Inceo-

This work was supported by the National Institutes of Health National Institute of Environmental Health Sciences [Grants P42-ES04699, R01-ES002710] through the German Academic Exchange Service (DAAD, Bonn, Germany); and the American Asthma Foundation (to B.D.H.).

Article, publication date, and citation information can be found at http://dmd.aspetjournals.org.

http://dx.doi.org/10.1124/dmd.111.042283.

[S] The online version of this article (available at http://dmd.aspetjournals.org) contains supplemental material.

ABBREVIATIONS: TCC, 3,4,4′-trichlorocarbanilide; ACN, acetonitrile; CLM, cynomolgus monkey liver microsomes; I.S., internal standards; DCC, 4,4′-dichlorcarbanilide; DMSO, dimethyl sulfoxide; ESI, electrospray ionization; MS/MS, tandem mass spectrometry; MS, mass spectrometry; LC, liquid chromatography; HLM, human liver microsomes; HKM, human kidney microsomes; HIM, human intestine microsomes; MLM, mice liver microsomes; RLM, rat liver microsomes; SRM, selected reaction monitoring; UDPGA, UDP-diphosphoglucuronic acid; UGT, uridine-5′-diphosphate-glucuronosyltransferases.

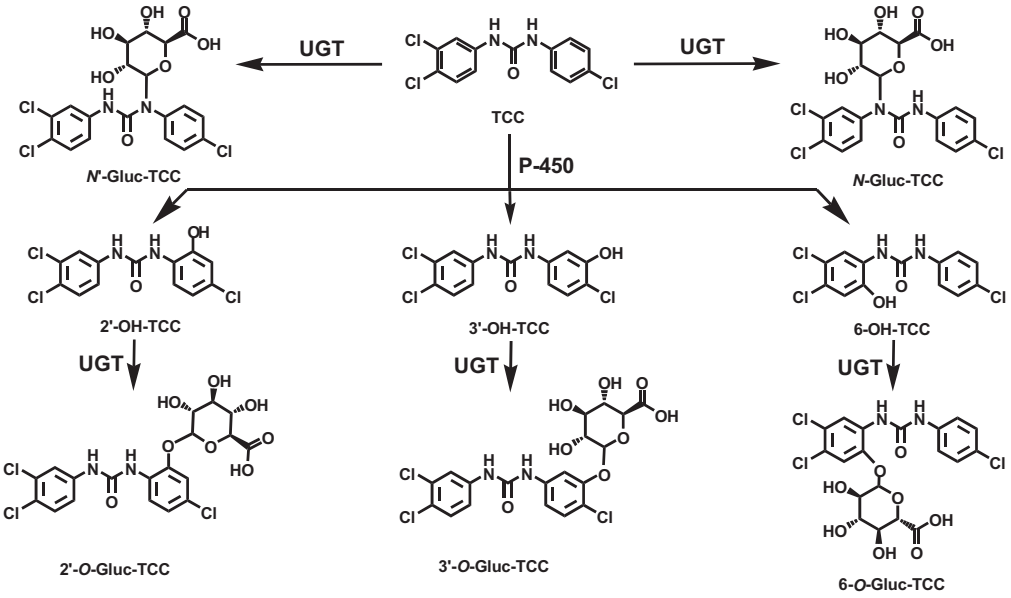

FIG. 1. Overview of the UGT-mediated TCC metabolism. Direct glucuronidation of TCC leads to *N*-glucuronides representing the major metabolites in human urine (Schebb et al., 2011c). The glucuronides of the oxidative metabolites 2′-OH-TCC, 3′-OH-TCC, and 6′-OH-TCC are the major metabolites in mammalian bile (Birch et al., 1978).

glu et al., 2011). In mammals, TCC is rapidly metabolized. The main metabolite detected in human and monkey urine, accounting for 25% of TCC elimination products, results from direct N-glucuronidation at one of the nitrogen atoms of the urea moiety of TCC (Birch et al., 1978; Hiles and Birch, 1978a; Hiles et al., 1978; Schebb et al., 2011c). The majority of absorbed TCC is metabolized by cytochrome P450 enzymes to three hydroxylated TCC species, namely 2′-OH-TCC, 3′-OH-TCC, and 6-OH-TCC (Hiles, 1977; Jeffcoat et al., 1977; Birch et al., 1978; Hiles and Birch, 1978a; Hiles and Birch, 1978b; Hiles et al., 1978; Warren et al., 1978) (Fig. 1) with the *ortho*-hydroxylated species, 2′-OH-TCC, and 6-OH-TCC as main metabolites (Birch et al., 1978). All metabolites undergo extensive phase II metabolism, and the glucuronic acid conjugates of the hydroxylated TCC species account for the majority of TCC metabolites in mammalian bile (Birch et al., 1978). Thus, conjugation with glucuronic acid plays a key role in both renal and biliary elimination of TCC. In a recent study, it was also shown that glucuronides of phase I metabolites are the major metabolites in fish (Schebb et al., 2011a). However, no information is available about the UDP-glucuronosyltransferases (UGTs) involved in the conjugation of TCC and its metabolites, as well as the biochemistry and kinetics of the conversion. Therefore, in this study we investigated the activity of liver, kidney, and intestinal microsomes, and individual human UGT for the conjugation of TCC and its oxidative metabolites. Moreover, the enzyme kinetics for the glucuronidation of 2′-OH-TCC by liver microsomes was evaluated to obtain quantitative data about the clearance of this metabolite.

Materials and Methods

Chemicals. TCC was purchased from Sigma-Aldrich (St. Louis, MO) and further purified (≥99.9%) by repeated recrystallization. The TCC metabolites 2′-OH-TCC, 3′-OH-TCC, 6-OH-TCC, and 2′-Gluc-TCC, and the internal standards (I.S.) 4,4′-dichlorcarbanilide (DCC) and 2′-SO_3-*O*-TCC were synthesized by coupling the appropriate isocyanate and amine compounds, as described previously (Ahn et al., 2008; Baumann et al., 2010). The chemical structures of the analytes are shown in Fig. 1. Uridine 5′-diphosphoglucuronic acid (UDPGA) trisodium salt, alamethicin, and D-saccharolactone were obtained from Sigma-Aldrich. All other chemicals were from Thermo Fisher Scientific (Waltham, MA) and were of the highest quality available.

Microsomes and Human UGT Isoforms. All microsomes and Supersomes, i.e., microsomes from insect Sf9 cells infected with a baculovirus strain containing cDNA of human UGT isoforms, were obtained from BD Gentest (Woburn, MA). The following microsomal preparations were used (20 mg · protein^{-1} · ml^{-1}): pooled human liver microsomes (HLM) from 25 mixed-gender donors, pooled rat liver microsomes (RLM) from 150 male Sprague-Dawley rats, pooled mouse liver microsomes (MLM) from 100 male B6C3F1 mice, pooled cynomolgus monkey liver microsomes (CLM) from 13 male animals, pooled human kidney microsomes (HKM) from mixed-gender donors, and pooled human intestine microsomes (HIM) from 10 mixed-gender donors. Supersomes of the following human UGT isoforms were used: UGT1A1, UGT1A3, UGT1A4, UGT1A6, UGT1A7, UGT1A8, UGT1A9, UGT1A10, UGT2B4, UGT2B7, UGT2B15, and UGT2B17. The activity of the microsomal preparations was verified by monitoring their ability to conjugate the standard UGT substrates 4-(trifluoromethyl) umbelliferone (TFMU) and trifluoperazine. The measured activities using the respective substrates are shown in the supplemental data.

Glucuronidation Assays. The glucuronidation assay was performed as described by Maul et al. (2011) with slight modifications (Pfeiffer et al., 2006, 2009). Microsomes or individual UGTs were incubated with TCC and its hydroxylated metabolites in a total volume of 200 μl of 100 mM potassium phosphate buffer (pH 7.4). In a generic scheme, 20 μl of microsome solution containing 5 μg of protein were mixed with 76 μl of buffer and 40 μl of alamethicin solution (125 μg/ml) and placed on ice for 15 min. Alamethicin forms pores in the microsomal membrane and increases the substrate accessibility of the UGTs (Fisher et al., 2000). Subsequently, 4 μl of the substrate in dimethyl sulfoxide (DMSO; concentration in assay 10 μM, 2% DMSO), magnesium chloride, and the β-glucuronidase inhibitor saccharolactone (concentration in assay both 10 mM) were added, and the mixture was preincubated for 5 min at 37°C on a heated shaker. The reaction was initiated by the addition of 20 μl of UDPGA (20 mM) and incubated for an additional 30 min. After 5, 10, 15, and 30 min (for highly active preparations: 2, 5, 10, and 15 min), 40-μl samples were transferred from each incubation mixture to a vial with 40 μl of acetonitrile (ACN) containing I.S. The final I.S. concentration was 1 μM. DCC was used as IS for the incubations of TCC, 2′-OH-TCC, and 6-OH-TCC. 2′-SO_3-*O*-TCC served as I.S. for incubations of 3′-OH-TCC. The resulting suspension was vigorously mixed and centrifuged at 16,000*g* for 10 min to remove precipitated protein and buffer salts. The supernatant was directly used for liquid chromatography-UV-electrospray ionization-tandem mass spectrometry (LC-UV-ESI-MS/MS) analysis.

For the determination of the 2′-OH-TCC glucuronidation kinetics, various substrate concentrations (0.2, 0.5, 1, 2, 3, 5, 10, and 50 μM) were incubated with RLM, HLM, CLM, and MLM for 5, 10, 15, and 30 min, respectively. To keep the concentration of all samples within the linear range of the ESI-MS/MS detection, samples containing ≥5 μM substrate were mixed 1:9 with ACN after incubation. Control incubations were conducted either in the absence of UDPGA or with Supersomes lacking an active UGT isoform in the

presence of UDPGA. Each incubation was carried out in three independent replicates.

LC-UV-MS Analysis. LC-UV-ESI-MS/MS analysis was performed using Waters Premier system (Waters, Milford, MA). Separation was performed on an RP-18 column with embedded polar groups of the dimensions 2 × 100 mm and a particle size of 2.2 μm (ProntoSIL C18 ace-EPS; BISCHOFF Chromatography, Leonberg, Germany). The analytes (injection volume 10 μl) were separated by a binary gradient at a flow rate of 300 μl/min of 25 mM ammonium acetate containing 0.1% acetic acid as solvent A and pure ACN as solvent B. The following gradient was used: 0.0 to 2.0 min isocratic 30% B, 2.0 to 7.5 min nonlinear with decreasing slope [convex gradient curve profile; MassLynx (Waters) software setpoint 5] 30 to 85% B, 7.5 to 8.5 min linear 80 to 100% B, 8.5 to 9.5 min isocratic 100% B, 9.5 to 9.7 min return to initial conditions of 30% B, and reconditioning between 9.7 and 11.0 min. Analytes were detected using a UV detector operating at 265 nm and negative ESI MS/MS in sensitive and specific selected reaction monitoring (SRM) mode. MS/MS conditions for TCC, 2′-OH-TCC, 3′-OH-TCC, 6-OH-TCC, 2′-Gluc-*O*-TCC, 2′-SO_3-*O*-TCC, and DCC were optimized by infusing 100 nM of a solution of analytes in 80:20 ACN/water at a flow rate of 10 μl/min with a syringe pump. The optimization of separation and detection conditions for the further glucuronides was performed with biological samples because no standard substances were available. Human urine (diluted 1:1 with ACN and centrifuged) of an exposed subject was used as source of the two *N*-glucuronides, as described previously (Schebb et al., 2011c). 3′-Gluc-*O*-TCC and 6-Gluc-*O*-TCC were generated by microsomal incubations with RLM, as described above. The optimized MS conditions and fragment spectra of the glucuronides are shown in the supplemental data (Table S1; Fig. S1).

The activity of the microsomes and individual UGTs was calculated based on the amount of formed product. For 2′-Gluc-*O*-TCC, the quantification was performed by external calibration of the LC-UV-MS signal. The concentration of the other glucuronides was calculated based on their peak areas in the UV signal using the calibration function of their substrates. It is assumed that the glucuronides have the same molar absorbance as their aglycones.

The conversion rate was determined by linear regression of at least three data points of the product formation over the incubation time. Activity values were calculated based on the linear regression as mean and S.D. of three independent incubations. The K_M and V_{max} values for the glucuronidation of 2′-OH-TCC were obtained by fitting the conversion rates versus the concentration according to eq. 1 with the SigmaPlot (version 9.01; Systat Software, Inc., San Jose, CA).

$$v = \frac{V_{max} \times c}{K_M + c} \quad (1)$$

In Vivo Experiments. To verify the formation of the glucuronides in vivo, urine of rodents was analyzed in a preliminary metabolism study. Two 12-week-old male Sprague-Dawley rats (Charles River Laboratories, Inc., Wilmington, MA) with a body weight of 458 ± 25 g and two 12-week-old male Swiss Webster mice (Charles River Laboratories, Inc.) of 34.4 ± 0.7 g were used. This study was approved by the University of California (UC) Davis Institutional Animal Care and Use Committee. Before the experiment, animals were housed in UC Davis facilities with access to food and water ad libitum. Animals were transferred into metabolic cages 24 h before the experiment (Pakenham et al., 2002) and blank urine was collected. Two mice were placed in one metabolic cage and each rat was housed in a single cage. TCC was administered by oral gavage of a 1 mg/ml solution of TCC in 20:80 DMSO/PEG400 (v/v). Rats received a dose of 1 mg/kg b.wt., and mice received a dose of 5 mg/kg b.wt. After administration, urine was collected between 0 to 24 and 24 to 48 h. Urine was analyzed using online-LC-MS, as described previously (Schebb et al., 2011a).

Results

LC-UV-MS Method. The glucuronidation of TCC and its three monohydroxylated metabolites was investigated using different microsomes and individual UGTs. To quantitatively monitor the conjugate formation, analytical methods are needed to quantify the product formation. Therefore, a new LC-UV-MS method was developed. The application of an RP-column with embedded polar groups and 2.2-μm particles yielded in a high-chromatographic resolution allowing a separation of TCC and all its metabolites in only 8 min (Fig. 2A). For the metabolites with available reference standards, 2-Gluc-TCC (peak

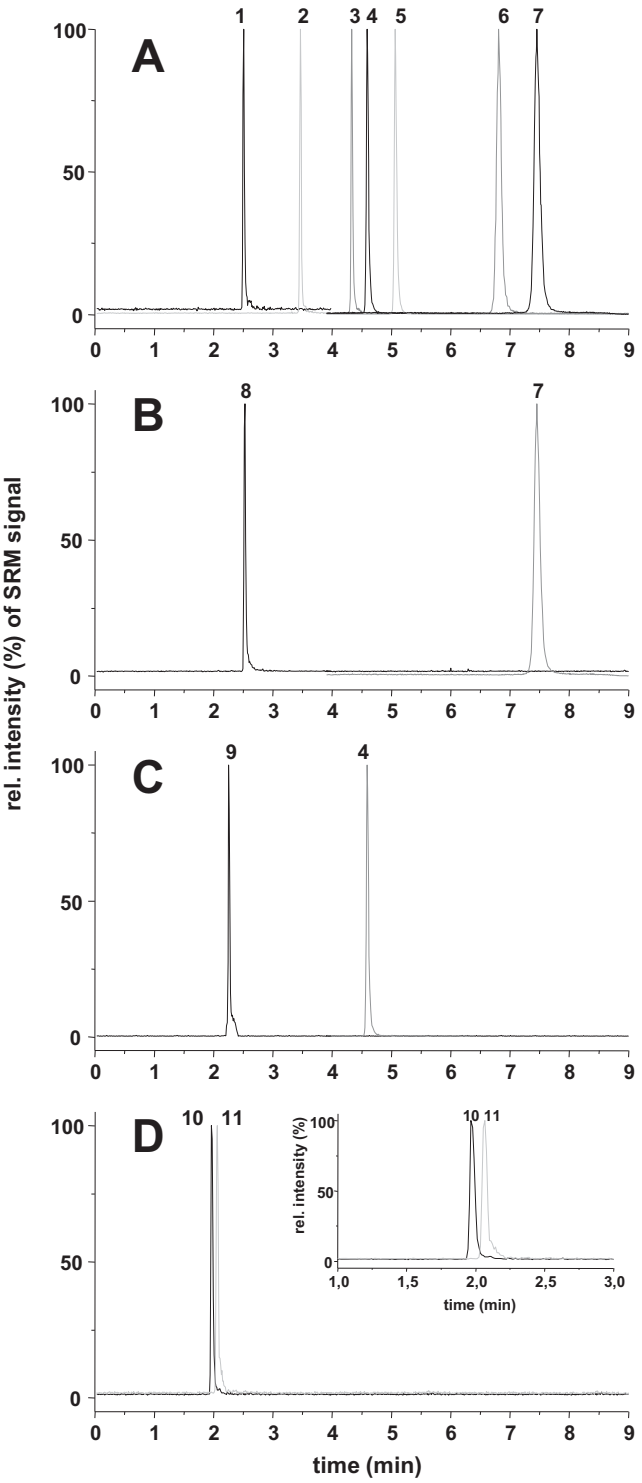

FIG. 2. Chromatographic separation with ESI-MS detection in SRM mode of TCC and its metabolites. Shown is an injection of a standard solution (50 nM) (A), 40-min microsomal conversion of 6-OH-TCC (10 μM) (B) with RLM and 3′-OH-TCC (10 μM) (C) with RLM microsomes (0.025 mg protein/ml). D, analysis of a urine sample of a TCC exposed human is displayed. The peaks in the SRM chromatograms are 2′-*O*-gluc-TCC (1), 2′-SO_3-*O*-TCC (2), DCC (I.S.) (3), 3′-OH-TCC (4), TCC (5), 2′-OH-TCC (6), 6-OH-TCC (7), 6-*O*-gluc-TCC (8), 3′-*O*-gluc-TCC (9), *N*-Gluc-TCC (10), and *N*′-Gluc-TCC (11).

1) eluted first, followed by the sulfate conjugate of 2′-OH-TCC, 2′-SO_3-*O*-TCC (peak 2), used as IS. At a retention time of 4.61 min, 3′-OH-TCC eluted (peak 3), closely followed by the I.S. DCC (peak 4) and TCC (peak 5). In contrast to earlier attempts for a reversed-phase separation (Birch et al., 1978; Baumann et al., 2010), the metabolites hydroxylated in ortho position to the urea moiety. 2′-OH-TCC (peak 6) and 6-OH-TCC (peak 7) were also baseline separated and eluted at 6.81 min and 7.45 min, respectively. The prolonged retention time of these hydroxylated metabolites compared with TCC can be explained by the formation of an intermolecular hydrogen bond between the hydroxyl and urea group (Birch et al., 1978; Warren et al., 1978; Baumann et al., 2010; Schebb et al., 2011c). Incubation of 3′-OH-TCC with RLM in the presence of UDPGA led to an abundant peak at 2.26 min (Fig. 2), which caused $[M-H]^-$ ions with *m/z* of 505, 507, and 509. The pattern of these ions indicated a compound containing three chlorine atoms. In addition, the fragment spectrum of this metabolite showed the same fragments as 2′-Gluc-*O*-TCC and was therefore tentatively identified as the 3′-Gluc-*O*-TCC. After incubation of 6-OH-TCC with RLM and UDPGA, peak 9 with a retention time of 2.51 min was detected. Showing the same isotopic pattern of the parent $[M-H]^-$ ions as 2′-Gluc-*O*-TCC and 3′Gluc-*O*-TCC, the formed metabolite showed intense fragment ions at *m/z* 202, which is characteristic for the isocyanate fragment ions of TCC derivatives bearing a hydroxyl function in the dichloroaniline ring (Baumann et al., 2010; Schebb et al., 2011c) (Supplemental Fig. S1). To optimize the method with respect to the *N*-glucuronides of TCC, urine of a human subject that had been exposed to TCC was used as a source of *N*′-Gluc-TCC and *N*-Gluc-TCC for these conjugates (Fig. 1) (Schebb et al., 2011c). The *N*-Gluc-TCC eluted at 1.97 min and was almost baseline separated from *N*′-Gluc-TCC with a retention time of 2.07 min (Fig. 2).

All five glucuronic acid conjugates showed the same characteristic fragmentation of the urea backbone as previously described for TCC and its phase I metabolites (Baumann et al., 2010; Schebb et al., 2011c) (Supplemental Fig. S1; Table S1). Using these fragments for detection in SRM mode, TCC and all its metabolites could be specifically monitored. The method showed a high sensitivity with a detection limit of 3 fmol on column for most of the compounds (Table 1). Due to the narrow peak width, the detection limit in UV detection at 265 nm of 0.1 μM (300 fmol on column) was also relatively low. In UV detection, the slopes of 0.7 and 0.6 of the calibration curve for 2′-*O*-Gluc-TCC and its aglycone 2′-OH-TCC were very similar. Based on this difference of <15%, it was assumed that all TCC glucuronic acid conjugates show the same molar absorbance as their corresponding aglycones. Therefore, further quantification of the glucuronides was performed based on the LC-UV calibration of their parent compounds.

The sensitivity of the LC-UV-MS method allowed us to evaluate the product formation at four time points over the incubation time of a single incubation sample with a volume of 0.2 ml. The conversion rate for each incubation was calculated using linear regression of the product formation versus incubation time. This yields a more precise determination of the initial enzyme velocity than those values derived from common endpoint assays, which assume a linear product formation over the entire incubation time (Pfeiffer et al., 2006, 2009; Maul et al., 2011). The formation of all measured products was linear over an incubation time of 20 min or longer, and at least three data points of product formation were used for the linear regression. For highly active preparations and low product concentrations in the kinetic measurements, the incubation time was reduced and samples were taken at 2, 5, 10, and 15 min.

Activity Screening for the Conjugation of TCC and Its Metabolites. The activity of various enzyme preparations for the conjugation of TCC and its oxidative metabolites was investigated using microsomes from different species and different tissues to enable estimation of the tissues in which the glucuronidation may occur in vivo. To compare the activity of the microsomal preparations at their V_{max}, this activity screening was performed at a high substrate concentration of 10 μM, which is above the expected K_M. As shown in Table 2, the liver microsomes of the four mammalian species tested, namely HLM, CLM, RLM, and MLM, showed a high activity of at least 3 nmol · min^{-1} · mg $protein^{-1}$ for the conjugation of the three hydroxylated TCC metabolites. The glucuronidation activity for 2′-OH-TCC of HLM, RLM, and MLM was very similar (mean 2.63 ± 0.06 nmol · min^{-1} · mg $protein^{-1}$). Conjugation of 3′-OH-TCC and 6-OH-TCC occurred at a 2- to 3-fold higher rate, with remarkable species-dependent differences. Whereas 3′-OH-TCC was conjugated most extensively by RLM and MLM, HLM showed the highest activity for the conjugation of 6-OH-TCC. CLM showed higher activities for all hydroxylated TCC metabolites than the microsomes of the other species. Here, 2′-OH-TCC was conjugated the fastest, with an activity of 23 nmol · min^{-1} · mg $protein^{-1}$, followed by 6-OH-TCC and 3′-OH-TCC. Microsomes from human, kidney and intestine overall showed a comparable activity to HLM for the conjugation of the three monohydroxylated TCC metabolites. It is interesting to note that the activity of HIM and HKM to conjugate 2′-OH-TCC was higher (5.62 ± 0.06 nmol · min^{-1} · mg $protein^{-1}$) compared with HLM, whereas 3′-OH-TCC and 6-OH-TCC were glucuronidated at equal or

TABLE 1

Performance of the analytical method

Retention time, limit of detection, and linear range ($R^2 \geq 0.99$) for ESI-MS detection in SRM mode, and UV detection at 265 nm are shown.

Compound	Retention Time	LC-ESI(−)-MS/MS		UV	
		LOD	LOQ Linear Range	LOD	LOQ Linear Range
	min	*fmol*	*nM*	*fmol*	*nM*
DCC	4.36 ± 0.03	3	1–1000	300	100–10,000
TCC	5.10 ± 0.04	3	1–1000	300	100–10,000
2′-OH-TCC	6.81 ± 0.07	3	1–1000	300	100–10,000
6′-OH-TCC	7.45 ± 0.05	3	1–1000	300	100–10,000
3′-OH-TCC	4.61 ± 0.02	3	1–1000	300	100–10,000
2′-SO_3-*O*-TCC	3.46 ± 0.02	3	1–1000	300	100–10,000
N-Gluc-TCC	1.97 ± 0.01	n.d.	n.d.	n.d.	n.d.
N′-Gluc-TCC	2.07 ± 0.02	n.d.	n.d.	n.d.	n.d.
2′-*O*-gluc-TCC	2.50 ± 0.02	10	3–1000	300	100–10,000
6′-*O*-gluc-TCC	2.51 ± 0.02	n.d.	n.d.	n.d.	n.d.
3′-*O*-gluc-TCC	2.26 ± 0.02	n.d.	n.d.	n.d.	n.d.

LOQ, limit of quantitation; n.d., not determined because no reference compound was available.

TABLE 2

Activities of various microsomes and human UGT-isoforms for the glucuronidation of 2′-OH-TCC, 3′-OH-TCC, 6-OH-TCC, and TCC determined by LC-UV (265 nm)

Activities are expressed as pmol · min^{-1} · mg $protein^{-1}$ as the mean and S.D. of three independent measurements.

Microsomes/UGT-Isoform	2′-OH-TCC	6-OH-TCC	3′-OH-TCC	TCC	
				N-Gluc	*N′*-Gluc
RLM	2600 ± 130	5500 ± 1800	8700 ± 2800	n.d.	n.d.
HLM	2700 ± 680	8500 ± 2200	5200 ± 150	n.d.*,+	n.d.*,++
CLM	22800 ± 100	16300 ± 700	9500 ± 1500	n.d.*,++	n.d.*,++
MLM	2600 ± 650	7900 ± 2400	14700 ± 690	n.d.*,++	n.d.*,++
HKM	5600 ± 1700	7700 ± 610	4200 ± 30	n.d.*,+++	n.d.*,+++
HIM	5700 ± 1200	3900 ± 1400	7100 ± 600	n.d.	n.d.
1A1	850 ± 210	820 ± 260	520 ± 20	n.d.	n.d.
1A3	390 ± 93	410 ± 50	540 ± 70	n.d.	n.d.
1A4	n.d.	n.d.	n.d.	n.d.	n.d.
1A6	n.d.	n.d.	n.d.*	n.d.	n.d.
1A7	870 ± 440	1100 ± 320	1700 ± 160	n.d.	n.d.
1A8	5700 ± 2200	5000 ± 1100	9400 ± 250	n.d.	n.d.
1A9	1200 ± 800	2400 ± 680	840 ± 190	n.d.*,+	n.d.*,++
1A10	210 ± 160	280 ± 150	<LOQ	n.d.	n.d.
2B4	n.d.	n.d.*	n.d.	n.d.	n.d.
2B7	<LOQ	<LOQ	n.d.*	n.d.	n.d.
2B15	n.d.	n.d.	n.d.	n.d.	n.d.
2B17	n.d.	n.d.	n.d.	n.d.	n.d.

<LOQ (limit of quantitation), glucuronide peak < LOQ of LC-UV detection (0.2 μM); n.d. (not determined because no reference compound was available), glucuronide peak < LOQ of LC-UV detection (60 nM).

* Low product amounts detected by ESI-MS.

+, ++, +++, The activity for the N-glucuronidation is rated semiquantitatively [from low (+) to high (+++)] based on the peak height in the ESI-MS signal.

lower rates. Under similar conditions, none of the tested microsomes formed significant *N*-Gluc-TCC or *N′*-Gluc-TCC amounts, even at elevated protein concentrations up to 2 mg/ml in the microsomal incubations (Table 2). It is not likely that the absence of *N*-glucuronides can be explained by degradation during or after incubation, because similar investigations demonstrated that these metabolites are stable in urine and water ACN mixtures (Schebb et al., 2011c).

The SRM-ESI-MS signal showed a low formation of *N*-Gluc-TCC and *N′*-Gluc-TCC in HLM, CLM, MLM, and HKM incubations (Supplemental Fig. S2); however, no signals were observed in LC-UV chromatogram. Thus, quantification was not feasible, and the activity of the microsomes to glucuronidate TCC was estimated semiquantitatively based on the peak height in LC-MS (Table 2). HKM showed the highest activity, followed by MLM, CLM, and HLM. RLM incubations did not lead to any formation of TCC-*N*-glucuronides. Likewise, none of the isolated UGTs (Supersomes) showed activity for TCC glucuronidation, except for UGT1A9, which caused small *N*-glucuronide peaks in LC-ESI-MS (Supplemental Fig. S2). Even in incubations with elevated microsomal protein concentration (up to 2 mg/ml), none of the other UGTs formed detectable levels of *N*-glucuronides in a 30-min incubation. By contrast, a broad variety of human UGTs showed high activities for the conjugation of the three hydroxylated TCC metabolites. Here, UGT1A7, UGT1A8, and UGT1A9 were most active with activities of 1 nmol · min^{-1} · mg $protein^{-1}$ and higher. The extrahepatic UGT1A8 showed the strongest formation of glucuronides of all three phase I metabolites, being most active for transforming 3′-OH-TCC, followed by 2′-OH-TCC (Table 2). The less active UGT1A9 showed a different substrate selectivity and conjugated the metabolites in the order 6-OH-TCC, >2′-OH-TCC, >3′-OH-TCC, whereas UGT1A7 showed very similar activities on all compounds between 1.0 and 1.5 nmol · min^{-1} · mg $protein^{-1}$. UGT1A1, UGT1A3, and UGT1A10 had moderate activities for the conjugation of the hydroxylated TCC. UGT1A4, UGT1A6, and none of the tested enzymes of the UGT2 family showed significant activity for the glucuronidation of TCC and its metabolites.

To estimate the clearance of 2′-OH-TCC in the liver, its conjugation kinetics were investigated in different liver microsomes. Product formation was linear for at least three of the four incubation times investigated. For all four species, the conjugation followed Michaelis-Menten-type kinetics, as indicated by a linear correlation in the Lineweaver-Burk and Eadie-Hofstee plots (shown for CLM in Supplemental Fig. S3). A K_M in the low μM range was calculated for the liver microsomes of the four mammalian species. RLM, HLM, and MLM showed a similar K_M between 2.5 and 3.3 μM (Table 3), whereas CLM showed a significantly lower K_M of 1.4 ± 0.9 μM. The V_{max} of 26.7 ± 4.8 nmol · min^{-1} · mg $protein^{-1}$ was dramatically higher in CLM than in the other species, with 5.37 ± 0.43 nmol · mg^{-1} · min^{-1} for HLM, 9.42 ± 4.8 nmol · min^{-1} · mg $protein^{-1}$ for RLM, and 1.45 ± 0.43 nmol · min^{-1} · mg $protein^{-1}$ for MLM. It should be noted that the activity of CLM for the model substrate 4-(trifluoromethyl) umbelliferone was also approximately 2-fold higher than that of RLM, MLM, and HLM. Thus, the calculated high V_{max} might be caused by a higher UGT content in CLM compared with the other mammalian liver microsomes. Based on this kinetics, a similar intrinsic clearance of approximately 1.5 ml · min^{-1} · mg $protein^{-1}$ of 2′-OH-TCC was calculated for humans and mice. RLM and, particularly, CLM show higher clearance of the oxidative TCC metabolites (Table 3).

The analysis of mouse and rat urine after oral administration confirmed earlier studies that glucuronides are the major renal excretion form of TCC (Fig. 3). As described by Birch et al. (1978), no *N*-glucuronides were detected in the rat urine, and we found that the glucuronide of 3′-OH-TCC was the major urinary metabolite. By contrast, this study showed that mice form *N* and *N′*-glucuronides as major urinary metabolites similar to humans and monkeys. In addition, glucuronides of hydroxylated species were detected, indicating that at doses of 1 to 5 mg/kg b.wt. [a high dose compared with the human exposure caused by soaps of approximately 1 μg/kg b.wt. (Schebb et al., 2011c)], these metabolites contribute to the renal clearance of TCC (Fig. 3).

Discussion

The particular importance of a conjugation with glucuronic acid for the excretion of TCC in mammals has been known for more than 30

TABLE 3

K_M and V_{max} values for the glucuronidation of 2′-OH-TCC by the UGTs of different microsomes determined by LC-ESI-MS

Mean and S.D. of three independent measurements are shown. Internal clearance for each tissue was calculated based on these results.

Microsomes	K_M	V_{max}	Clearance
	μM	$nmol \cdot min^{-1} \cdot mg^{-1}$	$ml \cdot min^{-1} \cdot mg^{-1}$
RLM	3.29 ± 0.89	9.42 ± 4.80	2.86 ± 1.46
HLM	3.08 ± 1.37	5.37 ± 0.43	1.74 ± 0.31
CLM	1.40 ± 0.90	26.7 ± 4.80	19.1 ± 5.33
MLM	2.46 ± 0.19	1.45 ± 0.16	0.59 ± 0.16

years (Birch et al., 1978). However, this study is the first investigation of the biochemical formation of these glucuronides. By performing microsomal incubations in combination with a new LC-MS method, we showed that various human UGTs rapidly glucuronidate the TCC phase I metabolites 2′-OH-TCC, 3′-OH-TCC, and 6-OH-TCC.

The hepatic UGTs (UGT1A1, UGT1A3, and UGT1A9) (King et al., 2000; Tukey and Strassburg, 2000) showed high activities for the conjugation of all hydroxylated metabolites. The highest activity was found for UGT1A9, which favored 6-OH-TCC as substrate, followed by 2′-OH-TCC and 3′-OH-TCC. As expected from these results, HLM showed high activity for the conjugation of the hydroxylated TCC metabolites, with a descending conversion rate order of 6-OH-TCC >3′-OH-TCC >2′-OH-TCC. Rapid conjugation of the oxidative TCC metabolites was also found in the liver microsomes of mouse, monkey, and rat, indicating that mammalian liver UGTs generally show a high affinity for hydroxylated TCC metabolites. This is consistent with in vivo observations, where glucuronides of hydroxylated TCC species are by far the dominant metabolites found in mammalian bile (Birch et al., 1978).

The UGTs 1A1, 1A3, and 1A9 possessing high activity for the conversion of hydroxylated TCC are also expressed in other organs, such as the kidney and gastrointestinal tract (King et al., 2000; Tukey and Strassburg, 2000). Our activity screening also unveiled very high conjugation activity for the extrahepatic UGTs 1A7 and 1A8 (Table 2). Thus, it is concluded that oxidative TCC metabolites will also be rapidly conjugated in other tissues. This assumption is supported by the investigation of microsomes of kidney and intestine, which conjugated oxidative TCC metabolites at rates comparable with HLM. The substrate selectivity pattern of HKM was 6-OH-TCC >2′-OH-TCC >3′-OH-TCC, consistent with the pattern of the highly active UGT1A9, which is expressed in the kidney (Tukey and Strassburg, 2000). Likewise, HIM conjugated 3′-OH-TCC the fastest, followed by 2′-OH-TCC and 6-OH-TCC, which is identical to the pattern observed for the intestinal UGT1A8 (Tukey and Strassburg, 2000). None of the enzymes of the UGT2 family showed significant activity for the conjugation of phase I TCC metabolites.

Recent studies indicate that further oxidation of 2′-OH-TCC leads to a reactive quinone imine metabolite that covalently binds to proteins in vitro (Baumann et al., 2010). The formation of significant amounts of free 2′-OH-TCC may be of concern for human health. Therefore, we investigated the kinetics of the glucuronidation of 2′-OH-TCC as a possible detoxifying reaction in mammalian liver microsomes competing with a further cytochrome P450 oxidation. All tested microsomes showed a low K_M and a high V_{max}, resulting in a high apparent intrinsic clearance (Table 3). The clearance of 2′-OH-TCC by MLM and RLM was comparable or higher than the reported values for reference UGT substrates including 4-methylumbelliferone, *para*-nitrophenol, propofol, and mycophenolic acid (Shiratani et al., 2008). With a conversion rate of 1.74 $ml \cdot mg^{-1} \cdot min^{-1}$, the clearance of HLM was also significantly higher than for estradiol and its catecholic oxidative metabolites, which are believed to play a role in estradiol-mediated carcinogenesis (Pfeiffer et al., 2006). However, because both *N*- and *O*-glucuronides can be cleaved by glucuronidase from *Escherichia coli* (Schebb et al., 2011c), enterohepatic circulation will probably occur for biliary-excreted TCC metabolites.

Aside from oxidative metabolism with subsequent conjugation, direct N-glucuronidation is a major pathway in the metabolism and excretion of TCC (Fig. 1) (Birch et al., 1978). Humans excrete approximately 25% of the total absorbed TCC in the urine as *N*- and *N′*-glucuronide (Scharpf et al., 1975; Schebb et al., 2011c). These metabolites are also the major urinary TCC metabolites in monkeys and in mice, whereas no N-glucuronidation was observed in rats (Fig. 3) (Birch et al., 1978). According to this species specificity, TCC-*N*-glucuronides were detected after incubation with HLM, CLM, and MLM, but not after incubation with RLM. However, none of the microsomal incubations showed a formation of TCC-*N*-glucuronides at a rate higher than 1%. We therefore have to conclude that microsomal incubations poorly predict the in vivo importance of this metabolic pathway. There are two possible explanations for this observation: TCC-N-glucuronidation in vivo is catalyzed by other glucuronosyltransferases than the UGTs present in the microsomes; or TCC-N-glucuronidation by UGT does not occur to the same extent in vitro than it occurs in vivo. There is some evidence favoring the latter explanation. First, there are several studies that showed N-glucuronidation reactions are underestimated by microsomal incubations (Anderson et al., 2009). In particular, TCC is not well metabolized in microsomal incubations, as shown for oxidative metabolic conversions (Baumann et al., 2010). However, earlier findings show that the structurally similar carbanilide sorafenib, bearing more polar groups at both aniline rings than TCC, is converted by HLM to *N*-glucuronides at significant conversion rates (Sparidans et al., 2009). Therefore, urea derivatives, bearing a phenyl moiety on both nitrogen atoms, have to be regarded as possible substrates for UGT.

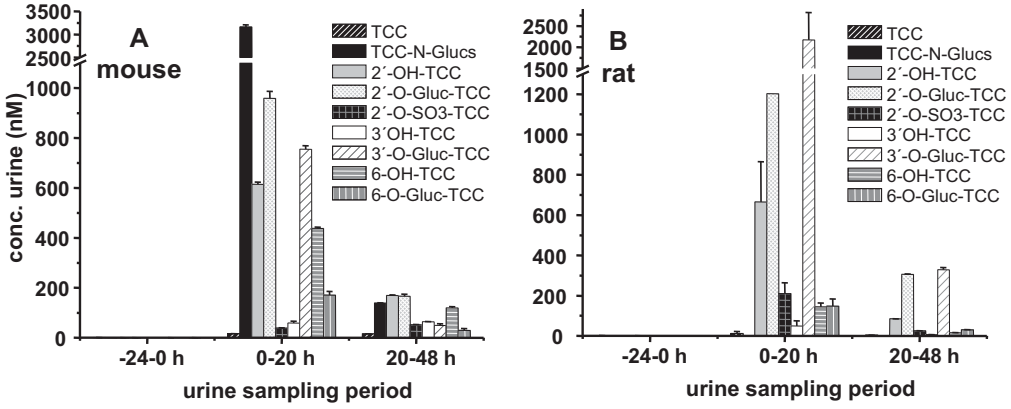

FIG. 3. Metabolic pattern of the TCC metabolites in rodent urine. A, the TCC metabolite concentration in mouse urine after oral gavage of 5 mg/kg b.wt. (t = 0 h) is shown. Results are shown as mean and S.D. of two independent experiments. B, TCC metabolites in rat urine after oral gavage of 1 mg/kg b.wt. (t = 0 h) are depicted. Results are shown as mean and S.D. of 3-fold analysis of the combined urine of two animals.

In the activity screening that used human UGTs, only incubations with UGT1A9 caused significant, although low, levels of *N*-glucuronides. The very low conversion rates did not allow a quantitative activity measurement. This observation indicates that it would be easy to overlook *N*-glucuronide formation by other isoforms. Therefore, the identification of UGT1A9 as the exclusive UGT catalyzing the N-glucuronidation of TCC should be confirmed by more predictive models consistent with the high conjugation rates found in vivo. For this purpose, metabolic studies using cell lines, precision tissue slices, transgenic animals transfected with human UGT isoforms, or the UGT1$^{-/-}$ mouse model could be beneficial. Optionally, enzyme-specific inhibitors could be used in the cell culture experiments. Nevertheless, the tentative identification of UGT1A9 as being the key enzyme in TCC-N-glucuronidation provides a convincing explanation for the observed species selectivity of this metabolic pathway. Whereas human, monkey, and mouse express an active enzyme, UGT1A9 is a pseudogene in rat (Mackenzie et al., 2005). Consequently, only incubation with RLM did not lead to any *N*-glucuronides in our experiments. With respect to tissue specificity, the observed activity of HLM, HIM, and HKM is also in accordance with the expression pattern of UGT1A9 being expressed in all these tissues (Ohno and Nakajin, 2009). Finally, the conjugation of the urea-nitrogen in TCC is consistent with the substrate specificity of UGT1A9. For example, UGT1A9 is the key enzyme for the formation of the ternary *N*-hydroxy-PhIP-*N*3-glucuronide (Malfatti and Felton, 2001) and for the N-glucuronidation of the structurally similar *para*-ethoxy phenyl urea (Uesawa et al., 2007).

In summary, our study showed that all major oxidative metabolites of TCC are rapidly conjugated with glucuronic acid by microsomes from liver, kidney, and intestine. A broad variety of UGTs have high affinity for the hydroxylated TCC metabolites, with high activities particularly for UGT1A7, UGT1A8, and UGT1A9. By contrast, hardly any *N*-glucuronides of TCC are formed in microsomal incubations. Nevertheless, based on sensitive LC-ESI-MS detection of low amounts of the formed product, UGT1A9 could be tentatively identified as a major UGT in this metabolic pathway of TCC.

Acknowledgments

We thank Robert Tukey and Mei-Fei Yueh (University of California, San Diego) for helpful discussions.

Authorship Contributions

Participated in research design: Schebb and Hammock.

Conducted experiments: Schebb and Franze.

Contributed new reagents or analytic tools: Schebb, Franze, Maul, and Ranganathan.

Performed data analysis: Schebb, Franze, and Maul.

Wrote or contributed to the writing of the manuscript: Schebb, Franze, Maul, Ranganathan, and Hammock.

References

Ahn KC, Zhao B, Chen J, Cherednichenko G, Sanmarti E, Denison MS, Lasley B, Pessah IN, Kültz D, Chang DP, et al. (2008) In vitro biological activities of the antimicrobials triclocarban, its analogues, and triclosan in bioassay screens. Receptor-based bioassay screens. *Environ Health Perspect* **116:**1203–1210.

Anderson S, Luffer-Atlas D, and Knadler MP (2009) Predicting circulating human metabolites: how good are we? *Chem Res Toxicol* **22:**243–256.

Baumann A, Lohmann W, Rose T, Ahn KC, Hammock BD, Karst U, and Schebb NH (2010) Electrochemistry-mass spectrometry unveils the formation of reactive triclocarban metabolites. *Drug Metab Dispos* **38:**2130–2138.

Birch CG, Hiles RA, Eichhold TH, Jeffcoat AR, Handy RW, Hill JM, Willis SL, Hess TR, and Wall ME (1978) Biotransformation products of 3,4,4′-trichlorocarbanilide in rat, monkey, and man. *Drug Metab Dispos* **6:**169–176.

Chen J, Ahn KC, Gee NA, Ahmed MI, Duleba AJ, Zhao L, Gee SJ, Hammock BD, and Lasley BL (2008) Triclocarban enhances testosterone action: a new type of endocrine disruptor? *Endocrinology* **149:**1173–1179.

Coogan MA, Edziyie RE, La Point TW, and Venables BJ (2007) Algal bioaccumulation of triclocarban, triclosan, and methyl-triclosan in a North Texas wastewater treatment plant receiving stream. *Chemosphere* **67:**1911–1918.

Coogan MA and La Point TW (2008) Snail bioaccumulation of triclocarban, triclosan, and methyltriclosan in a North Texas, USA, stream affected by wastewater treatment plant runoff. *Environ Toxicol Chem* **27:**1788–1793.

Fisher MB, Campanale K, Ackermann BL, VandenBranden M, and Wrighton SA (2000) In vitro glucuronidation using human liver microsomes and the pore-forming peptide alamethicin. *Drug Metab Dispos* **28:**560–566.

Halden RU and Paull DH (2005) Co-occurrence of triclocarban and triclosan in U.S. water resources. *Environ Sci Technol* **39:**1420–1426.

Hiles RA (1977) Metabolism and toxicity of halogenated carbanilides: absorption, distribution and excretion of radioactivity from 3,4,4′-trichloro[14C]carbanilide (TCC) and 3-trifluoromethyl-4,4′-dichloro[14C]carbanilide (TFC) in rats. *Food Cosmet Toxicol* **15:**205–211.

Hiles RA and Birch CG (1978a) The absorption, excretion, and biotransformation of 3,4,4′-trichlorocarbanilide in humans. *Drug Metab Dispos* **6:**177–183.

Hiles RA and Birch CG (1978b) Nonlinear metabolism and disposition of 3,4,4′-trichlorocarbanilide in the rat. *Toxicol Appl Pharmacol* **46:**323–337.

Hiles RA, Caudill D, Birch CG, and Eichhold T (1978) The metabolism and disposition of 3,4,4′-trichlorocarbanilide in the intact and bile duct-cannulated adult and in the newborn rhesus monkey (M. mulatta). *Toxicol Appl Pharmacol* **46:**593–608.

Imig JD and Hammock BD (2009) Soluble epoxide hydrolase as a therapeutic target for cardiovascular diseases. *Nat Rev Drug Discov* **8:**794–805.

Inceoglu B, Jinks SL, Schmelzer KR, Waite T, Kim IH, and Hammock BD (2006) Inhibition of soluble epoxide hydrolase reduces LPS-induced thermal hyperalgesia and mechanical allodynia in a rat model of inflammatory pain. *Life Sci* **79:**2311–2319.

Inceoglu B, Wagner K, Schebb NH, Morisseau C, Jinks SL, Ulu A, Hegedus C, Rose T, Brosnan R, and Hammock BD (2011) Analgesia mediated by soluble epoxide hydrolase inhibitors is dependent on cAMP. *Proc Natl Acad Sci USA* **108:**5093–5097.

Jeffcoat AR, Handy RW, Francis MT, Willis S, Wall ME, Birch CG, and Hiles RA (1977) The metabolism and toxicity of halogenated carbanilides. Biliary metabolites of 3,4,4′-trichlorocarbanilide and 3-trifluoromethyl-4,4′-dichlorocarbanilide in the rat. *Drug Metab Dispos* **5:**157–166.

King CD, Rios GR, Green MD, and Tephly TR (2000) UDP-glucuronosyltransferases. *Curr Drug Metab* **1:**143–161.

Mackenzie PI, Bock KW, Burchell B, Guillemette C, Ikushiro S, Iyanagi T, Miners JO, Owens IS, and Nebert DW (2005) Nomenclature update for the mammalian UDP glycosyltransferase (UGT) gene superfamily. *Pharmacogenet Genomics* **15:**677–685.

Malfatti MA and Felton JS (2001) N-glucuronidation of 2-amino-1-methyl-6-phenylimidazo[4,5-b]pyridine (PhIP) and N-hydroxy-PhIP by specific human UDP-glucuronosyltransferases. *Carcinogenesis* **22:**1087–1093.

Maul R, Siegl D, and Kulling SE (2011) Glucuronidation of the red clover isoflavone irilone by liver microsomes from different species and human UDP-glucuronosyltransferases. *Drug Metab Dispos* **39:**610–616.

Morisseau C, Merzlikin O, Lin A, He G, Feng W, Padilla I, Denison MS, Pessah IN, and Hammock BD (2009) Toxicology in the fast lane: application of high-throughput bioassays to detect modulation of key enzymes and receptors. *Environ Health Perspect* **117:**1867–1872.

Ohno S and Nakajin S (2009) Determination of mRNA expression of human UDP-glucuronosyltransferases and application for localization in various human tissues by real-time reverse transcriptase-polymerase chain reaction. *Drug Metab Dispos* **37:**32–40.

Pakenham G, Lango J, Buonarati M, Morin D, and Buckpitt A (2002) Urinary naphthalene mercapturates as biomarkers of exposure and stereoselectivity of naphthalene epoxidation. *Drug Metab Dispos* **30:**247–253.

Pfeiffer E, Graf E, Gerstner S, and Metzler M (2006) Stimulation of estradiol glucuronidation: a protective mechanism against estradiol-mediated carcinogenesis? *Mol Nutr Food Res* **50:**385–389.

Pfeiffer E, Schmit C, Burkhardt B, Altemöller M, Podlech J, and Metzler M (2009) Glucuronidation of the mycotoxins alternariol and alternariol-9-methyl ether in vitro: chemical structures of glucuronides and activities of human UDP-glucuronosyltransferase isoformes. *Mycotox Res* **25:**3–10.

Sapkota A, Heidler J, and Halden RU (2007) Detection of triclocarban and two co-contaminating chlorocarbanilides in US aquatic environments using isotope dilution liquid chromatography tandem mass spectrometry. *Environ Res* **103:**21–29.

Scharpf LG Jr, Hill ID, and Maibach HI (1975) Percutaneous penetration and disposition of triclocarban in man: body showering. *Arch Environ Health* **30:**7–14.

Schebb NH, Flores I, Kurobe T, Franze B, Ranganathan A, Hammock BD, and Teh S (2011a) Bioconcentration, Metabolism and Excretion of Triclocarban in larval Qurt Medaka (Oryzias latipes). *Aquat Toxicol* **105:**448–454.

Schebb NH, Huby M, Morisseau C, Hwang SH, and Hammock BD (2011b) Development of an online SPE-LC-MS-based assay using endogenous substrate for investigation of soluble epoxide hydrolase (sEH) inhibitors. *Anal Bioanal Chem* **400:**1359–1366.

Schebb NH, Inceoglu B, Ahn KC, Morisseau C, Gee SJ, and Hammock BD (2011c) Investigation of human exposure to triclocarban after showering and preliminary evaluation of its biological effects. *Environ Sci Technol* **45:**3109–3115.

Shiratani H, Katoh M, Nakajima M, and Yokoi T (2008) Species differences in UDP-glucuronosyltransferase activities in mice and rats. *Drug Metab Dispos* **36:**1745–1752.

Sparidans RW, Vlaming ML, Lagas JS, Schinkel AH, Schellens JH, and Beijnen JH (2009) Liquid chromatography-tandem mass spectrometric assay for sorafenib and sorafenib-glucuronide in mouse plasma and liver homogenate and identification of the glucuronide metabolite. *J Chromatogr B Analyt Technol Biomed Life Sci* **877:**269–276.

Tukey RH and Strassburg CP (2000) Human UDP-glucuronosyltransferases: metabolism, expression, and disease. *Annu Rev Pharmacol Toxicol* **40:**581–616.

Uesawa Y, Staines AG, Lockley D, Mohri K, and Burchell B (2007) Identification of the human liver UDP-glucuronosyltransferase involved in the metabolism of p-ethoxyphenylurea (dulcin). *Arch Toxicol* **81:**163–168.

Warren JT, Allen R, and Carter DE (1978) Identification of the metabolites of trichlorocarbanilide in the rat. *Drug Metab Dispos* **6:**38–44.

Address correspondence to: Bruce D. Hammock, University of California, Davis, Department of Entomology, One Shields Ave., Davis, CA 95616. E-mail: bdhammock@ucdavis.edu